Compact, stable 1 ghz femtosecond er-doped fiber lasers

Citation: Hyunil Byun, Michelle Y. Sander, Ali Motamedi, Hanfei Shen, Gale S. Petrich, Leslie A. Kolodziejski, Erich P. Ippen, and Franz X. Kärtner, "Compact, stable 1 GHz femtosecond Er-doped fiber lasers," Appl. Opt. 49, 5577-5582 (2010)

As Published: http://dx.doi.org/10.1364/AO.49.005577

Publisher: Optical Society of America

Persistent URL: http://hdl.handle.net/1721.1/72009

Version: Author's final manuscript: final author's manuscript post peer review, without publisher's formatting or copy editing

Compact, stable 1 GHz femtosecond Er-doped fiber lasers

Hyunil Byun*, Michelle Y. Sander, Ali Motamedi, Hanfei Shen, Gale S. Petrich, Leslie A. Kolodziejski, Erich P. Ippen and Franz X. Kärtner

Department of Electrical Engineering and Computer Science, and Research Laboratory of Electronics,

Massachusetts Institute of Technology, 77 Massachusetts Avenue, Cambridge, Massachusetts 02139, USA

Corresponding author: hibyun@mit.edu

We demonstrate a high-repetition-rate soliton fiber laser that is based on highly-doped anomalously-dispersive erbium-doped fiber. By splicing an 11-mm single mode fiber to the erbium-doped fiber, thermal damage of the butt-coupled saturable Bragg reflector (SBR) is overcome. The laser generates 187-fs pulses at a repetition rate of 967 MHz with a measured long-term stability of more than 60 hours.

OCIS codes: 320.7110 (Ultrafast nonlinear optics), 320.5550 (pulses), 140.3538 (lasers, pulsed)

1. Introduction

High repetition rate femtosecond lasers are needed for applications such as optical arbitrary waveform generation [1], frequency metrology [2] and high speed optical sampling [3]. A successful approach to obtaining compact fiber laser cavities [4-6] is based on passive mode-locking with a saturable Bragg reflector (SBR) [7-10] butt-coupled to a fiber cavity with net

negative dispersion to enable soliton pulse shaping [10, 11]. Such fundamentally mode-locked lasers are attractive femtosecond pulse sources for low timing jitter applications because of their simplicity and low cost. To successfully scale these lasers towards higher repetition rates while maintaining the needed soliton pulse shaping, one needs to take into account the reduced pulse energy, the reduced peak power and the smaller nonlinear phase shifts and intracavity dispersion resulting from the shorter gain fiber lengths [12].

Femtosecond pulses at wavelengths around 1.55 μm were generated at a repetition rate near 500 MHz in a cavity with the gain fiber butt-coupled to the SBR [4]. Fiber lasers with repetition rates up to 2 GHz were reported by McFerran et al. [5]. However, these lasers operated in a picosecond pulse regime and with an average output power of 1.3 mW. Recent experimental demonstrations of fiber lasers mode-locked with SBRs achieved repetition rates as high as 3 GHz [6], but with similarly low efficiency; with 700 mW of pump power only 2 mW of output power was measured. Additionally, thermal damage to the SBR was found to limit the long-term stability of the mode-locked laser output. When the gain fiber is butt-coupled to the SBR, the hot fiber core is in direct contact with the SBR and the SBR's surface experiences intense thermal heating. This can eventually result in failure of the laser after a short period of operation. Minimizing the thermal damage is therefore particularly important for high-repetition-rate fiber lasers to ensure long-term stable operation. Carbon nanotube fiber lasers with a repetition rate of 5 GHz and a pulse duration of 0.68 ps were demonstrated [7], but its timing jitter was much higher due to the longer pulses and lower intracavity pulse energy.

As an extension of earlier work [4], we report scaling fundamentally mode-locked fiber lasers to GHz repetition rates [13]. The challenge of thermal damage is addressed and a stable, efficient, low-jitter fiber laser with a repetition rate of 1 GHz is demonstrated. With the natural

recovery time of an InGaAs-based absorber in the SBR, a soliton femtosecond laser source with sub-200 fs pulses was constructed. The laser is thermally stable and has a very compact packaged footprint of 121×94×33 mm^3.

2. Experimental setup

The experimental setup for the erbium-doped fiber (EDF) laser is shown in Fig. 1. Fig. 1(a) outlines the laser schematic and illustrates the fiber assembly that separates the gain fiber from the SBR. The fiber section of the laser cavity consists of a 92-mm long Liekki Er80-8/125 erbium-doped gain fiber with anomalous dispersion of -20 fs^2/mm that was fusion-spliced to an 11-mm long piece of standard single-mode fiber (SMF-28e). Both ends of the fiber assembly are polished flat and the gain fiber is secured with epoxy in a 126-μm ID zirconia ferrule. Since the splice joint between the gain fiber and the SMF is slightly thicker than the bare gain fiber end, the SMF is secured with epoxy in a 127-μm ID zirconia ferrule. The SMF section is shorter than the ferrule so that the spliced section resides within the ferrule. A coated ferrule that is spliced to the wavelength division multiplexer (WDM), functions as a 10% output coupler and is connected to the gain fiber ferrule in a mating sleeve. With such a design, a very robust and relatively low-loss connection is obtained as compared to free space coupling of the pump into the gain fiber. Fig. 1(b) shows a photograph of the compact fiber laser package.

The SMF end of the fiber is butt-coupled to a III-V compound semiconductor SBR. Optical contact between the fiber tip and the SBR is confirmed by successful and stable modelocking, because an air layer between the fiber and the SBR would impair mode-locking by the etalon effect and cause increased cavity loss that would also lead to a considerable drop in laser efficiency. The SBR is used to facilitate the mode-locking and self-starting of the laser: a schematic of the SBR is illustrated in Fig. 2(a). The Bragg mirror, designed for a center

wavelength of 1550 nm, consists of a 22-pair quarter-wave stack of $Al_{0.95}Ga_{0.05}As$ and GaAs. On the surface of the high reflectivity mirror, the $In_{0.53}Ga_{0.47}As$ absorber is embedded in a half-wave cladding layer of GaAs. To reduce absorption of the residual pump power and to further minimize localized heating effects, a pump-reflective coating (PRC), consisting of Ti_3O_5 and SiO_2 with quarter–wave layer thicknesses centered at the pump wavelength, was deposited on the surface of the SBR. With this added dielectric coating, any unabsorbed pump power is reflected back into the gain fiber.

As seen in Fig. 2(b), the SBR exhibits a reflectivity of 95% at 1560 nm. The reflectivity is reduced to 88% after the deposition of the pump-reflective coating. Additionally, the added dielectric coating enhances the standing electric field at least by a factor of two, resulting in higher absorption losses and in a reduced saturation fluence. Fig. 2(c) shows the measured reflectivity of the saturable absorber without the pump-reflective coating as a function of the pump fluence at 1560 nm. The solid line is the result of the fit of a slow saturable-absorber model plus two-photon-absorption to the measured data. The data indicate that the SBR has a 4% saturable absorption, a 1% non-saturable loss and a saturation fluence of 11 $\mu J/cm^2$. The pump-probe measurements for delays of up to 50 ps show that the overall recovery time of the SBR is 9 ps (Fig. 2(d)). The group delay dispersion of the SBR with the PRC at a wavelength of 1568 nm is approximately -1300 fs^2 so that together with the anomalous dispersive gain fiber the cavity operates in a net negative dispersion regime that allows soliton formation.

3. Mode-locking results

Fig. 3 depicts the measured optical spectrum and interferometric autocorrelation (IAC) trace of the laser. The optical spectrum analyzer measurement shows a 17.5-nm full-width-half-maximum (FWHM) optical bandwidth, implying a 150-fs transform-limited FWHM pulse

duration. For the autocorrelation measurement, the laser output is amplified by an Er-doped fiber amplifier and followed by a dispersion compensating fiber (DCF) to compensate the dispersion in the measurement path. The autocorrelation measurement yields a 187-fs FWHM pulse duration (Fig. 3(b)). The difference can be attributed to a slightly imperfect dispersion compensation.

The optical spectrum is centered around 1573 nm, as determined by the wavelength-dependent reflectivity of the SBR and the gain spectrum at the operating power level. These values were obtained with 380 mW of pump power that was launched into the Er-fiber; the output signal power was measured to be 27.4 mW, which corresponds to 283-pJ intracavity pulse energy. An estimated 185 mW of the launched pump power is absorbed in the EDF core. Separate experiments show that 30% of the launched pump power is absorbed in a single pass through the gain fiber and 90% of the remaining pump is reflected by the butt-coupled SBR. The GHz laser was self-starting; with increasing pump power, the laser first operated in a Q-switched mode-locked state and then changed to a continuous-wave soliton mode-locked state at a pump power of 200 mW with a FWHM optical bandwidth of 9.0 nm. For a pump power greater than 382 mW, multiple pulsing occurred.

The 1-minute persistence trace, as seen in Fig. 3(d), shows excellent signal stability, while the RF spectrum in Fig. 3(c) indicates a signal-to-background ratio of 80 dB. Fig. 3(e) shows the single side band (SSB) phase noise of the first harmonic (967.3 MHz) of the laser. The laser output power is focused on a photodetector (EOTech ET-3500), filtered by a bandpass filter, and amplified to +16 dBm before being measured with the signal source analyzer (Agilent E5052). The timing jitter integrated from 10 MHz progressively down to 1 kHz is shown as a green dotted line, resulting in an integrated jitter of 22 fs over the entire interval. The phase noise

below 10 kHz follows a slope of -20 dBc/decade and can be suppressed by controlling the fiber length with a piezo-based stretcher and locking the repetition rate to an electronic oscillator with better long-term stability. The bandwidth limitations of this approach will likely limit the suppression of the phase noise to frequencies below ~10 kHz.

The relative intensity noise (RIN) is measured to demonstrate the stability of the output intensity. The laser output is converted to an electrical signal by an amplified InGaAs photodetector (Thorlabs PDA400) with a trans-impedance gain of 7500 V/A. The split output power level of 0.53 mW generated a voltage of 3.54 V at the detector output with a 50 Ω termination. The corresponding RIN of the shot noise level, -153 dBc/Hz, exceeds the noise floor of the vector signal analyzer (HP 89410A) so that the measured noise is purely contributed by the laser output noise and not limited by the vector signal analyzer. The integrated relative intensity noise of 0.014 % from 10 Hz to 10 MHz mostly originates from the pump diode noise that is shown as the black curve in Fig. 3(f). Note that the RIN of the laser is lower than that of the pump diode because the slope efficiency is reduced enough at the operation point due to gain saturation. A rapid drop of the laser RIN above 1 kHz is attributed to the long upper state lifetime of Er-ions. Both RINs of the pump diode and the laser show downward slopes near 7-8 MHz, which is consistent with detector 3-dB bandwidth of 10 MHz.

4. Thermal damage issue of SBR and long-term stability of laser

Increasing the pulse repetition rate of a soliton laser requires increasing the pump power so that the same pulse energy can be maintained for soliton formation [12]. Higher pump power leads to correspondingly more residual pump power at the other end of the fiber cavity and a higher fiber core temperature. With the EDF directly contacting the SBR, thermal damage was observed.

Four different configurations for the fiber cavity were evaluated to study the thermal damage issue (Fig. 4) that is related to the SBR. The EDF and the SBR are in direct contact with each other in configurations (a) and (b), while single-mode passive fiber (SMF-28e) is spliced to the EDF in configurations (c) and (d). The GaAs substrate of the SBR is 350-μm thick in configurations (a) and (c), while the substrate was lapped down to a final thickness of 150 μm in configurations (b) and (d) to improve heat sinking of the absorber layer. In all configurations, the total cavity length ranges from 100 mm to 105 mm, with a 6-mm long SMF section incorporated only for configurations (c) and (d). The mode-locking results described in section 3 above were obtained using the configuration shown in Figure 4(c) with a slightly longer length for the SMF section.

Configuration (a) was tested first. For a launched pump power of 180 mW, soliton pulses were generated with an optical spectrum FWHM width of 5.4 nm and an average output power of 5.0 mW at a repetition rate of 975 MHz. However, after tens of seconds, the output power dropped to a few nW, with permanently damage observed to the SBR and fiber ferrule. We assume that the hot fiber core may cause local deformation of the pump-reflective coating due to the different coefficients of thermal expansion between the dielectric coating and the underlying III-V compound semiconductor-based SBR. Following the deformation of the coating, the pump light may no longer be fully reflected and subsequently results in damage to the SBR by the heat generated from the absorbed pump. Using an approach similar to the report by Li [14], the core temperature can be estimated. According to our estimates, 185 mW of pump light is absorbed out of the 380 mW of launched pump power. Assuming that the pump is highly multi-mode and is absorbed uniformly over the core, the equivalent absorbed pump power with a prorated core diameter is 185 mW × (20 μm / 8 μm)^2 = 1.16 W. The equivalent launched pump power is thus

about two times the absorbed pump power, or 2.32 W, which raises the temperature of the core 55 °C above the ambient temperature. In this calculation, the same absorbed pump power per unit area is assumed to induce the same temperature increase of the core fiber.

To prevent thermal damage, two protective mechanisms were implemented in configuration (d): (1) the SBR substrate was thinned down and (2) the passive single mode fiber was inserted between the EDF and the SBR. The SMF lowers the heat transfer from the EDF core to the SBR and the thinned-down substrate facilitates heat transfer from the surface of the SBR to the copper mount. Employing both protective mechanisms, the laser demonstrated stable generation of soliton-like pulses for a tested time period exceeding three weeks.

Comparison of configurations (b) and (c), indicates that incorporating additional SMF has more impact than thinning the substrate of the SBR to prevent thermal damage as shown in Fig. 5. Without the added SMF, the output power continually drops to 70% of the starting power after 20 hours. In contrast, the SMF-buffered cavity maintains a constant output power with fluctuations of only a few percent, subsequently confirmed to be due to pump power fluctuations. The length of SMF used in configuration (c) was 6 mm.

The laser in section 3, based on configuration (c), was further investigated using active feedback control of the output power to negate pump power fluctuations. Fig. 6 shows the output power, the optical spectrum FWHM, the temperature inside the fiber package, and the repetition rate drift for 63 hours of operation. For a launched pump power of 270 mW, the output power is measured using a power meter with analog output, which records at a sampling rate of 1 sample per second through a data acquisition card (National Instrument PCI-6013). The optical spectral width and the repetition rate are transferred from the instruments (ANDO AQ6317 and HP 8568B, respectively) through GPIB interface every five seconds. For the active feedback, the

analog output of the power meter is fed into the negative input of a loop filter box (New Focus LB1005) and the loop filter output modulates the current of the pump diode driver.

Fig. 6(a) shows the output power over a period longer than two days with fluctuations of only 0.5%. The temperature in the laser package is also logged and shows a temperature cycle of 1.5 ºC each day. The measurement started at 10 am, and the temperature rise and fall occurs during daytime, while the temperature remains constant overnight. The optical spectral width and the repetition rate indicate good laser stability, with variations only slightly affected by the ambient temperature change. These temperature-dependent variations can be further reduced by better temperature control of the package.

The temperature-dependent optical spectrum can be explained by the fiber birefringence that varies with the ambient temperature. A single mode fiber supports two orthogonal polarization modes. In a perfectly circular fiber, the two polarization modes are degenerate, but generally fibers have slightly elliptical cross-section and possess birefringence, allowing different polarization components to interact with each other through nonlinear polarization coupling [15]. Depending on the cavity parameters including the fiber birefringence, the laser output polarization either evolves periodically or two polarization components are locked in phase to emit stable elliptically-polarized-solitons, called polarization-locked vector solitons (PLVS's) [16]. The polarization rotation can be eliminated by carefully aligning the fiber and operating the laser in the PLVS regime [17]. Whether the soliton is polarization-locked or not, the pulse energy changes with the fiber birefringence (see Fig. 2 in Ref. 15). The change of ambient temperature alters the birefringence of bent or twisted fibers [18] as noticed in our laser, and thus the pulse energy or the optical spectral width of the solitons.

The repetition rate drift of -7 ppm/ºC, as shown above, originates mostly from the temperature-dependent refractive index of the fiber. A higher temperature increases the optical path length of the laser cavity and reduces the repetition rate accordingly. The corresponding change of the optical path length, here +7 ppm/ºC, agrees well with the measured thermo-optic coefficients, dn/dT, of +8.5 ppm/ºC for fused silica fiber (Table 6 in Ref. [19]).

5. Conclusion

We demonstrated a monolithic, 1-GHz thermal-damage-free femtosecond fiber laser by inserting an undoped fiber piece between the gain fiber and the butt-coupled SBR. The laser, compactly packaged in a 121×94×33 mm^3 box, generates low-jitter 187-fs pulses at an output power level of 27.4 mW for 380 mW of launched pump power.

Acknowledgement

This work was supported in part by the Defense Advanced Research Projects Agency (DARPA) under Contract HR0011-05-C-0155 and Contract W911NF-04-1-0431, and in part by the Air Force Office of Scientific Research (AFOSR) under Contract FA9550-10-1-0063. The authors thank Peter O'Brien at MIT Lincoln Laboratory for deposition of the dielectric coatings on the SBRs.

References

1. D. J. Jones, S. A. Diddams, J. K. Ranka, A. Stentz, R. S. Windeler, J. L. Hall, and S. T.Cundiff, "Carrier-envelope phase control of femtosecond mode-locked lasers and direct optical frequency synthesis," Science **288**, 635 (2000).
2. S. T. Cundiff, "Metrology - New generation of combs," Nature **450**, 1175-1176 (2007).
3. J. Kim, M. Park, M. Perrott, and F. Kärtner, "Photonic subsampling analog-to-digital conversion of microwave signals at 40-GHz with higher than 7-ENOB resolution," Opt. Express **16**, 16509-16515 (2008).
4. H. Byun, D. Pudo, J. Chen, E. P. Ippen, and F. X. Kärtner, "High-repetition-rate, 491 MHz, femtosecond fiber laser with low timing jitter," Opt. Lett. **33**, 2221-2223 (2008).
5. J. J. McFerran, L. Nenadovic, W. C. Swann, J. B. Schlager, and N. R. Newbury, "A passively mode-locked fiber laser at 1.54 μm with a fundamental repetition frequency reaching 2 GHz," Opt. Express **15**, 13155-13166 (2007).
6. J. Chen, J. W. Sickler, H. Byun, E. P. Ippen, S. Jiang, and F. X. Kärtner, "Fundamentally Mode-locked 3 GHz Femtosecond Erbium Fiber Laser," in Ultrafast Phenomena XIV: Proceedings of the 16th International Conference (Italy, 2008), pp. 727-729.
7. S. Yamashita, Y. Inoue, K. Hsu, T. Kotake, H. Yaguchi, D. Tanaka, M. Jabronski, and S. Y. Set, "5GHz pulsed fiber Fabry-Perrot laser mode-locked using carbon nanotubes", IEEE Photonics Technol. Lett. **17**, 750-752 (2005).
8. H. A. Haus, "Theory of mode locking with a fast saturable absorber," J. Appl. Phys. **46**, 3049-3058 (1975).
9. R. Paschotta, U. Keller, "Passive mode locking with slow saturable absorbers," Appl. Phys. B **73**, 653-662 (2001).
10. F. X. Kärtner, J. Aus der Au, and U. Keller, "Mode-locking with slow and fast saturable absorbers – what's the difference?," IEEE J. Selected Topics in Quant. Electron. **4**, 159-168 (1998).
11. F. X. Kärtner and U. Keller, "Stabilization of solitonlike pulses with a slow saturable absorber," Opt. Lett. **20**, 16-18 (1995).
12. D. Pudo, H. Byun, J. Chen, J. Sickler, F. X. Kärtner, and E. P. Ippen, "Scaling of passively mode-locked soliton erbium waveguide lasers based on slow saturable absorbers," Opt. Express **16**, 19221-19231 (2008).
13. M. Y. Sander, H. Byun, J. Morse, D. Chao, H. M. Shen, A. Motamedi, G. Petrich, L. Kolodziejski, E. P. Ippen and F. X. Kärtner, "1 GHz femtosecond Erbium-doped fiber lasers," Conference on Lasers and Electro Optics (CLEO), San Jose, CA, May 16-21, 2010, CTuII1.
14. L. Li, H. Li, T. Qiu, V. L. Temyanko, M. M. Morrell, A. Schülzgen, A. Mafi, J. V. Moloney, and N. Peyghambarian, "3-Dimensional thermal analysis and active cooling of short-length high-power fiber lasers," Opt. Express **13**, 3420-3428 (2005).
15. D. N. Christodoulides and R. I. Joseph, "Vector solitons in birefringent nonlinear dispersive media," Opt. Lett. **13**, 53-55 (1988).
16. N. N. Akhmediev, J. M. Soto-Crespo, S. T. Cundiff, B. C. Collings, and W. H. Knox, "Phase locking and periodic evolution of solitons in passively mode-locked fiber lasers with a semiconductor saturable absorber," Opt. Lett. **23**, 852-854 (1998).
17. S. Cundiff, B. Collings, and W. Knox, "Polarization locking in an isotropic, modelocked soliton Er/Yb fiber laser," Opt. Express **1**, 12-21 (1997).

18. A. M. Smith, “Birefringence induced by bends and twists in single-mode optical fiber,” Appl. Opt. **19**, 2606-2611 (1980).
19. D. B. Leviton and B. J. Frey, “Temperature-dependent absolute refractive index measurements of synthetic fused silica,” Proc. SPIE **6273**, 62732K-11 (2006).

Figure caption

Fig. 1. (a) Laser schematic, (b) photograph of the packaged laser. The blue and red wires on the left side of the box are used to measure the temperature inside the package.

Fig. 2. (a) Schematic diagram of the SBR, (b) measured low-fluence reflectivity of the SBR over 900 nm to 1700 nm with and without the additional pump-reflective coating (PRC), (c) measured reflectivity of the SBR for various fluences at 1560 nm and (d) pump-probe traces for three different fluences. TPA: two photon absorption, $\Delta R/R$: relative reflectivity change.

Fig. 3. (a) Optical spectrum, (b) interferometric auto-correlation with inferred intensity autocorrelation (white), (c) RF spectrum zoomed around the first harmonic with a resolution bandwidth of 300 Hz, (d) 1-minute persistence trace, (e) single side band (SSB) phase noise and instrument noise floor with integrated timing jitter, and (f) relative intensity noise (RIN) of mode-locked EDF laser, pump diode and instrument noise floor.

Fig. 4. Four different configurations to study the thermal damage issue. EDF: Er-doped fiber, SBR: saturable Bragg reflector, and SMF: single mode fiber. All SBRs include the pump-reflective dielectric coatings deposited on the surface.

Fig. 5. 20-hour measurement of the output power for two different fiber cavity configurations.

Fig. 6. Long-term measurement of (a) output power, (b) temperature inside the package, (c) optical spectrum FWHM width, and (d) repetition rate drift from 967.398 MHz.

Figure 1

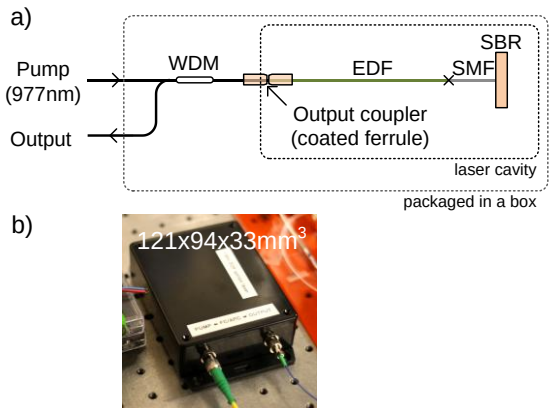
a)
Pump
(977nm)
Output
WDM
EDF
SBR
SMF
Output coupler
(coated ferrule)
laser cavity
packaged in a box
b)
121x94x33mm3

Figure 2

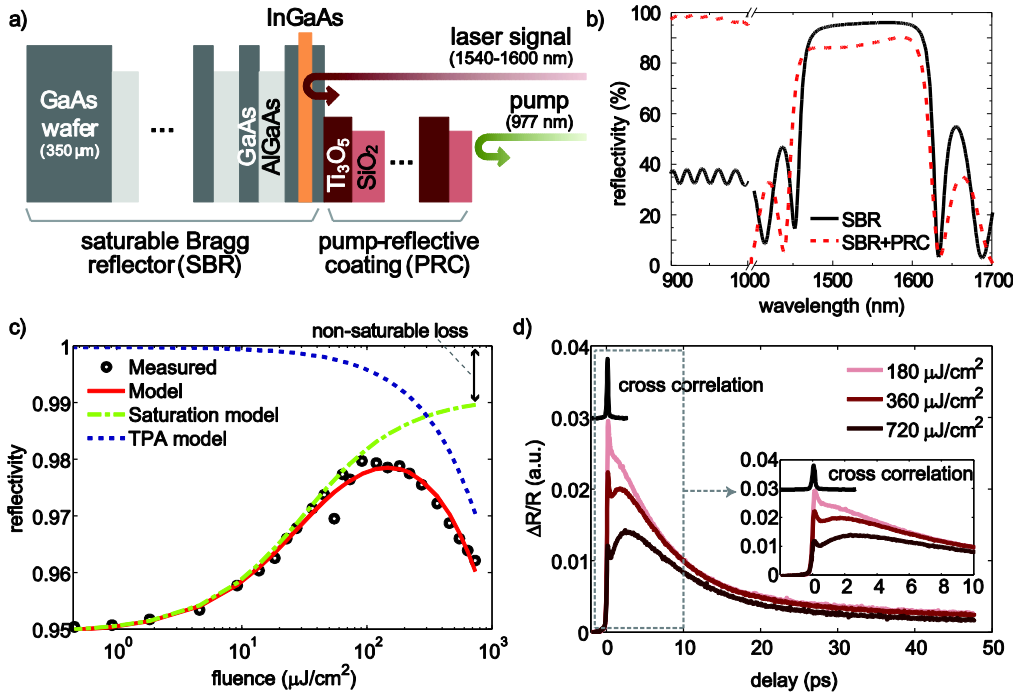
a)
InGaAs
laser signal
(1540-1600 nm)
pump
(977 nm)
GaAs
wafer
(350 μm)
GaAs
AlGaAs
Ti_3O_5
SiO_2
saturable Bragg
reflector (SBR)
pump-reflective
coating (PRC)
b)
reflectivity (%)
wavelength (nm)
SBR
SBR+PRC
c)
non-saturable loss
Measured
Model
Saturation model
TPA model
reflectivity
fluence (μJ/cm²)
d)
cross correlation
180 μJ/cm²
360 μJ/cm²
720 μJ/cm²
ΔR/R (a.u.)
delay (ps)

Figure 3

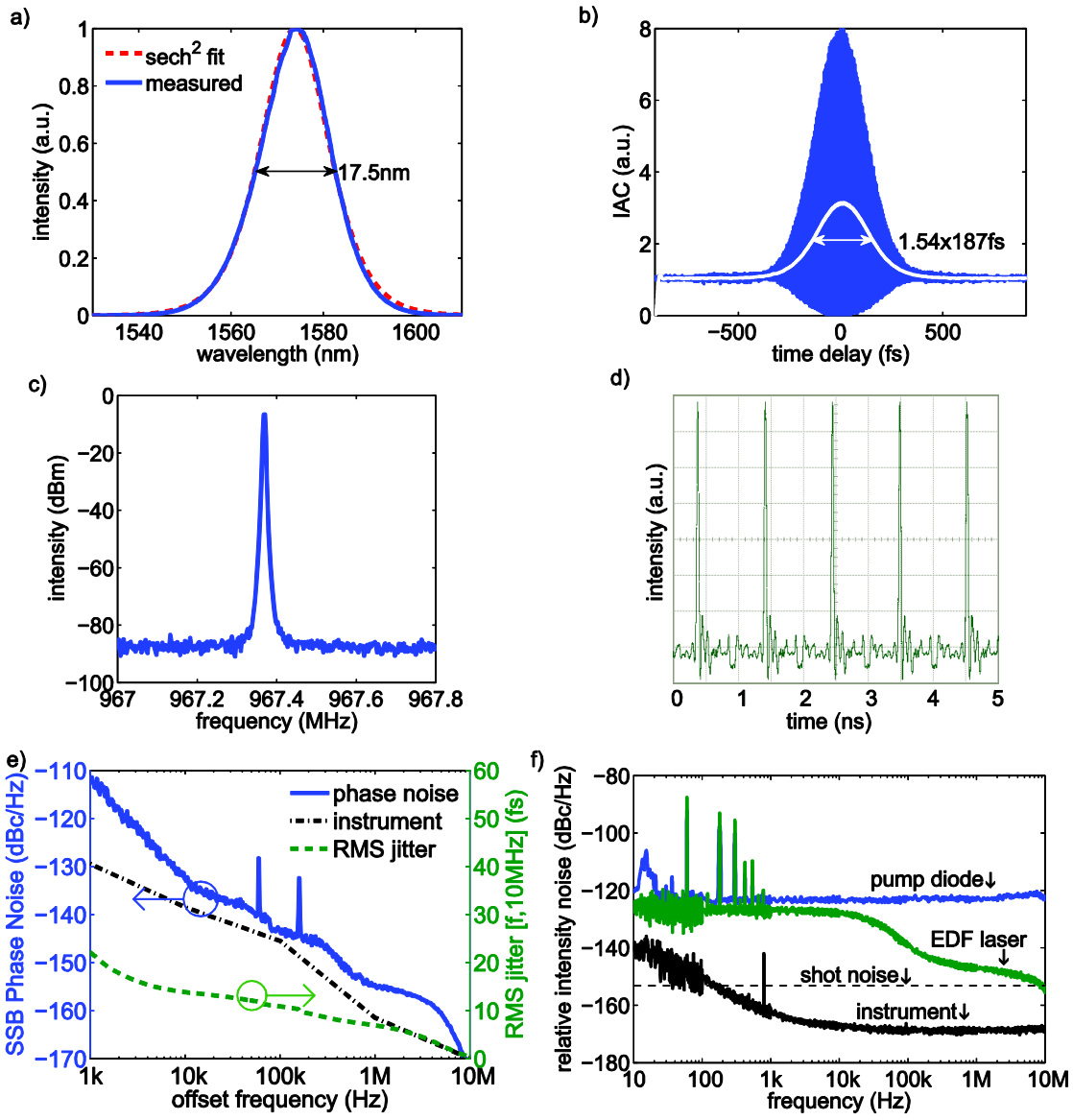
a)
sech2 fit
measured
17.5nm
intensity (a.u.)
wavelength (nm)
b)
IAC (a.u.)
1.54x187fs
time delay (fs)
c)
intensity (dBm)
frequency (MHz)
d)
intensity (a.u.)
time (ns)
e)
phase noise
instrument
RMS jitter
SSB Phase Noise (dBc/Hz)
RMS jitter [f,10MHz] (fs)
offset frequency (Hz)
f)
pump diode↓
EDF laser
shot noise↓
instrument↓
relative intensity noise (dBc/Hz)
frequency (Hz)

Figure 4

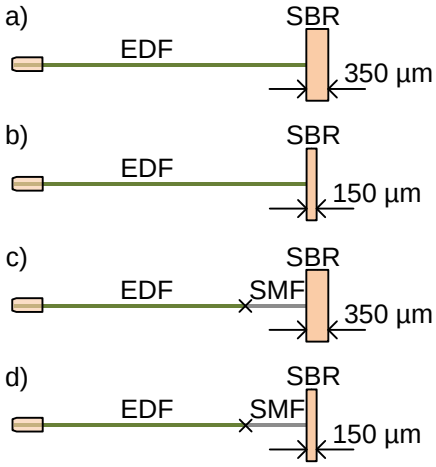
a)
SBR
EDF
350 µm
b)
SBR
EDF
150 µm
c)
SBR
EDF
SMF
350 µm
d)
SBR
EDF
SMF
150 µm

Figure 5

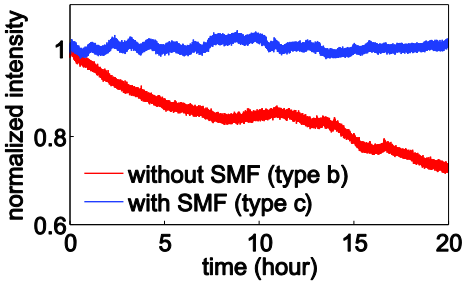
normalized intensity
1
0.8
0.6
0
5
10
15
20
time (hour)
without SMF (type b)
with SMF (type c)

Figure 6

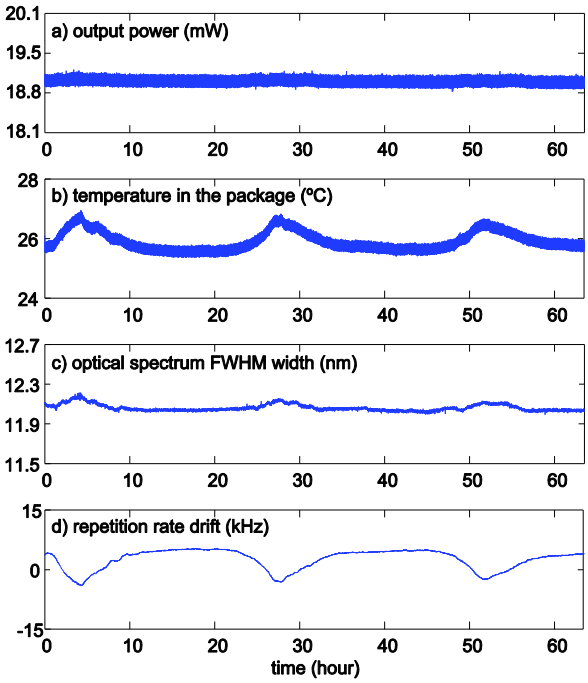
a) output power (mW)
20.1
19.5
18.8
18.1
b) temperature in the package (ºC)
28
26
24
c) optical spectrum FWHM width (nm)
12.7
12.3
11.9
11.5
d) repetition rate drift (kHz)
15
0
-15
0
10
20
30
40
50
60
time (hour)